

# Raman phonons as a probe of disorder, fluctuations and local structure in doped and undoped orthorhombic and rhombohedral manganites.

L. Martín-Carrón, A. de Andrés, M.J. Martínez-Lope, M.T. Casais and J.A. Alonso

*Instituto de Ciencia de Materiales de Madrid (Consejo Superior de Investigaciones Científicas) Cantoblanco, E-28049 Madrid, Spain*

(Received November 4, 2018)

We present a rationalization of the Raman spectra of orthorhombic and rhombohedral, stoichiometric and doped, manganese perovskites. In particular we study  $RMnO_3$  ( $R = La, Pr, Nd, Tb, Ho, Er, Y$  and  $Ca$ ) and the different phases of  $Ca$  or  $Sr$  doped  $RMnO_3$  compounds as well as cation deficient  $RMnO_3$ . The spectra of manganites can be understood as combinations of two kinds of spectra corresponding to two structural configurations of  $MnO_6$  octahedra and independently of the average structure obtained by diffraction techniques. One type of spectra corresponds to the orthorhombic  $Pbnm$  space group for octahedra with cooperative or dynamic Jahn-Teller distortions, with stretching modes as the main features and whose frequencies correlate to Mn-O distances. The other spectrum is associated to regular but tilted octahedra whose modes can be described in the rhombohedral  $R\bar{3}c$  structure, where only bending and tilt modes are observed. The main peaks of compounds with regular  $MnO_6$  octahedra, as  $CaMnO_3$ , highly  $Ca$  doped  $LaMnO_3$  or the metallic phases of  $Ca$  or  $Sr$  doped  $LaMnO_3$ , are bending and tilt  $MnO_6$  octahedra modes which correlate to  $R$ -O(1) bonds and Mn-O-Mn angles respectively. In low and optimally doped manganites, the intensity and width of the broad bands are related to the amplitude of the dynamic fluctuations produced by polaron hopping in the paramagnetic insulating regime. The activation energy, which is proportional to the polaron binding energy, is the measure of this amplitude. This study permits to detect and confirm the coexistence, in several compounds, of a paramagnetic matrix with lattice polaron together with regions without dynamic or static octahedron distortions, identical to the ferromagnetic metallic phase. We show that Raman spectroscopy is an excellent tool to obtain information on the local structure of the different micro or macro-phases present simultaneously in many manganites.

## I. INTRODUCTION

Manganese perovskites  $R_{1-x}A_x\text{MnO}_3$  ( $R$ = La or rare earth,  $A$ = Ca, Sr, Ba...) have recently attracted much interest because of their colossal magnetoresistance effect<sup>1</sup> that makes these systems promising for magnetic sensors and reading heads devices. In spite of the tremendous amount of published studies on this subject, many experimental facts are not well understood, or have to be reinterpreted. Theories do not give yet a quantitative description of, for example, the metal-insulator phase transition, but converge in the necessity to include electron-lattice interactions, which are able to localize the carriers into small polarons through their coupling to lattice distortions, disorder or phonons<sup>2</sup>. There is also large consensus on the importance of intrinsic inhomogeneities and phase coexistence that, in the optimally doped regime, can be visualized as polaron clusters in the ferromagnetic matrix and metallic clusters in the insulating phase<sup>3</sup>.

The phonons involved in the theories for these CMR systems are even stretching modes, like symmetric stretching (breathing mode), or antisymmetric stretching mode (Jahn-Teller (JT) mode)<sup>4</sup>. Both normal modes are identical to the lattice distortions achieved by  $\text{Mn}^{3+}$  ions in order to split the  $e_g$  electronic level (JT effect). It is therefore important to identify these phonons and study their behavior through the different structural phases and doping levels.

An anomalous frequency hardening and narrowing of the line-width of the tilt mode as the temperature decreases through the magnetic transition has been reported in  $\text{La}_{0.67}\text{Ca}_{0.33}\text{MnO}_3$  compound. This behaviour has been explained by a double exchange mechanism with electron-phonon coupling<sup>5</sup>. Liarokapis et al.<sup>6</sup> observed, for  $x \geq 0.4$ , the disappearance of the high frequency stretching modes in the  $\text{La}_{1-x}\text{Ca}_x\text{MnO}_3$  series. Granado et al.<sup>7</sup> report, in  $\text{La}_{1-x}\text{Mn}_{1-x}\text{O}_3$  The softening of the high frequency phonons across  $T_c$  and explained it to be caused by a strong spin-phonon coupling. On the other hand, the Raman background can give information of the electronic excitations. The change of the diffusive electronic Raman scattering in the paramagnetic phase has been attributed to the change from small to large polaron regimes across the para to ferromagnetic phase transition<sup>8,9</sup>.

The knowledge of the lattice vibrations and their correlation to the different phases, local order and conduction mechanisms is of crucial importance. A clear demonstration of this relation is the frustration of the insulator to metallic transition only by the isotope substitution of  $\text{O}^{16}$  by  $\text{O}^{18}$  in a  $\text{La}_{1/3}\text{Nd}_{1/3}\text{Ca}_{1/3}\text{MnO}_3$  compound<sup>10</sup>. But there is still controversy on the interpretation of the Raman spectra even for stoichiometric  $\text{RMnO}_3$  whose spectrum corresponds well to the expected normal modes for its orthorhombic structure<sup>11-13</sup>. The  $490 \text{ cm}^{-1}$  peak has been assigned to a bending<sup>11</sup> or to an asymmetric stretching<sup>6,14</sup>. Amelitchev et al.<sup>15</sup> studied the depen-

dence of the low frequency tilt mode with the tolerance factor, in many compounds. They assign the broad peaks (around  $490$  and  $610 \text{ cm}^{-1}$ ) in doped compounds to second order Raman scattering. Nevertheless, these authors state as remarkable the absence of the strong phonon lines near  $490$  and  $612 \text{ cm}^{-1}$  that dominate  $\text{LaMnO}_3$  while the modes below  $350 \text{ cm}^{-1}$  are preserved. A detailed Raman study of  $\text{CaMnO}_3$  has been published<sup>16</sup> during the publication process of the present work. We do not coincide with this assignment of the tilt and R modes (discussion in section IV-B). Björnsson et al.<sup>17</sup> observe two different sets of phonons in  $\text{La}_{0.8}\text{Sr}_{0.2}\text{MnO}_3$ , as well as the appearance of new narrow peaks in  $\text{La}_{0.9}\text{Sr}_{0.1}\text{MnO}_3$  at low temperatures. Their explanation for  $x=0.2$  is the existence of pronounced local orthorhombic distortions, in the rhombohedral structure, that vanish at low temperature. However, they cannot explain the evolution with temperature of the Raman spectra in the  $x=0.1$  compound. The Raman spectra of doped or non-stoichiometric manganites in their different structural and magnetic phases for all doping levels are not well understood.

In the present work we study orthorhombic stoichiometric  $\text{RMnO}_3$  ( $R$ = La, Pr, Nd, Tb, Ho, Er, Y and Ca) as well as A site doped or cation deficient orthorhombic or rhombohedral  $\text{RMnO}_3$  and for different doping levels.

## II. EXPERIMENTAL DETAILS

Polycrystalline  $\text{RMnO}_3$  ( $R$ = Pr, Nd, Tb, Ho, Er and Y) and  $\text{CaMnO}_3$  samples were obtained by citrate techniques. For  $R=\text{Pr}$  and  $\text{Nd}$ , the precursors were treated at  $1100^\circ\text{C}$  in a  $\text{N}_2$  flow for 12 h; annealing treatments in an inert atmosphere were necessary to avoid the formation of non-stoichiometric  $\text{Pr}(\text{Nd})\text{MnO}_{3+\delta}$  phases, containing a significant amount of  $\text{Mn}^{4+}$ . For  $R=\text{Tb}$ , the precursor powders were heated at  $1000^\circ\text{C}$  in air for 12 h. Finally, low temperature treatments were necessary for the samples with  $R=\text{Ho}$ ,  $\text{Y}$  and  $\text{Er}$ , to increase the yield of the orthorhombic phases, preventing or minimizing the stabilization of competitive hexagonal  $\text{RMnO}_3$  phases<sup>18</sup>. In the case of stoichiometric  $\text{LaMnO}_3$  a single crystal was available; it has been prepared by the floating zone method<sup>19</sup>. The rhombohedral  $\text{LaMnO}_{3+\delta}$  samples were prepared in polycrystalline form by a citrate technique as described elsewhere<sup>20</sup>, as well as  $\text{PrMnO}_{3+\delta}$ <sup>21</sup>.

Finally, Ca doped  $\text{LaMnO}_3$  compounds were prepared by the classical ceramic method by heating stoichiometric amounts of  $\text{La}_2\text{O}_3$ ,  $\text{MnO}_2$  and  $\text{CaCO}_3$  for 72 hours at  $1400^\circ\text{C}$ . Materials so obtained were quenched in air.

Raman spectra were obtained with a Jobin-Yvon HR 460 monochromator coupled to a liquid Nitrogen cooled CCD. The excitation light was the  $514.5 \text{ nm}$  line of a Spectra Physics Ar-Kr laser. The incident and scattered beams were focused using an Olympus microscope. A Kaiser SuperNotch filter was used to suppress the elastic

light. The laser power was reduced down to 0.1 mW (depending on the sample) in order to avoid the local heating of the samples at the laser spot. We used a continuous flow Oxford Instrument cryostat CF2102 to perform measurement from 10K to room temperature (RT).

### III. STRUCTURE AND NORMAL MODES

All the samples studied here present the same Pbnm ( $D_{2h}^{16}$ , with  $Z=4$ ) orthorhombic structure, except  $\text{La}_{0.7}\text{Sr}_{0.3}\text{MnO}_3$  and  $\text{LaMnO}_{3+\delta}$  that are rhombohedral with the  $\text{R}\bar{3}c$  ( $D_{3d}^6$ , with  $Z=2$ ) space group<sup>18,20,22</sup>. The Pbnm orthorhombic  $\text{RMnO}_3$  compounds are structurally distorted with respect to the cubic perovskite, in two ways: the  $\text{MnO}_6$  octahedra present a strong Jahn-Teller cooperative distortion due to  $\text{Mn}^{3+}$  ions, and the octahedra are tilted in order to optimize the R-O bond-lengths.  $\text{CaMnO}_3$  has the same Pbnm structure as the  $\text{RMnO}_3$  series but the Jahn-Teller distortion is negligible<sup>23</sup>. As doping  $\text{RMnO}_3$  with Ca or Sr the Jahn-Teller distortion decreases, as a consequence of the introduction of  $\text{Mn}^{4+}$  cations, and the structure becomes more regular, maintaining the tilting of the octahedra. For a broad range of Sr doping, or for oxygen deficient samples, the reported structure is rhombohedral with tilted octahedra and strictly identical Mn-O bonds<sup>22</sup>.

The Raman active modes of the Pbnm structure (the mirror plane 'm' is perpendicular to the long c-axis) are:  $7\text{A}_g + 7\text{B}_{1g} + 5\text{B}_{2g} + 5\text{B}_{3g}$ . Mn ions do not participate to any Raman mode, as they are located at inversion centers, while La and O(1) ions display the same kind of movements. These 24 Raman active modes can be classified into two symmetric and four antisymmetric stretching modes, four bending modes and six rotation and tilt modes of the octahedra. At last, eight modes are related to A site movements.

There are 30 normal modes at the zone center for the  $\text{R}\bar{3}c$  ( $Z=2$ ) rhombohedral structure  $\text{A}_{1g} + 3\text{A}_{2g} + 2\text{A}_{1u} + 4\text{A}_{2u} + 4\text{E}_g + 6\text{E}_u$ . Among these,  $1\text{A}_g + 4\text{E}_g$  are Raman active modes,  $3\text{A}_{2u} + 5\text{E}_u$  are IR active and the remaining  $2\text{A}_{1u} + 3\text{A}_{2g}$  are silent modes. For this structure, the Raman active modes can be classified into  $1\text{A}_{1g} + 1\text{E}_g$  rotational or tilt modes,  $1\text{E}_g$  bending and  $1\text{E}_g$  anti-stretching of the  $\text{MnO}_6$  octahedra, and the remaining  $\text{E}_g$  is related to a vibration of A ions<sup>24</sup>. The symmetric stretching mode is  $\text{A}_{2g}$  and therefore not observable.

### IV. RESULTS AND DISCUSSION

We discuss the assignment of the main Raman peaks of Ca doped and undoped  $\text{RMnO}_3$  orthorhombic compounds and explain the apparently different behavior of their frequencies. We have classified the manganese perovskites depending on the distortion of the Mn-O octahedra.  $\text{RMnO}_3$  compounds present a strong cooperative

JT distortion, a trivalent state for Mn ions, insulating behavior, high resistivity and are paramagnetic at RT. A second group corresponds to compounds with a negligible JT distortion either orthorhombic (as  $\text{CaMnO}_3$ , highly doped  $\text{La}_{1-x}\text{Ca}_x\text{MnO}_3$   $x \geq 0.5$  or the ferromagnetic metallic phase of  $x=0.33$  compound), or rhombohedral as  $\text{La}_{0.67}\text{Sr}_{0.33}\text{MnO}_3$ . At last we discuss the paramagnetic phase of the  $0 < x < 0.5$  compounds as well as non stoichiometric  $\text{RMnO}_3$  samples and phase coexistence.

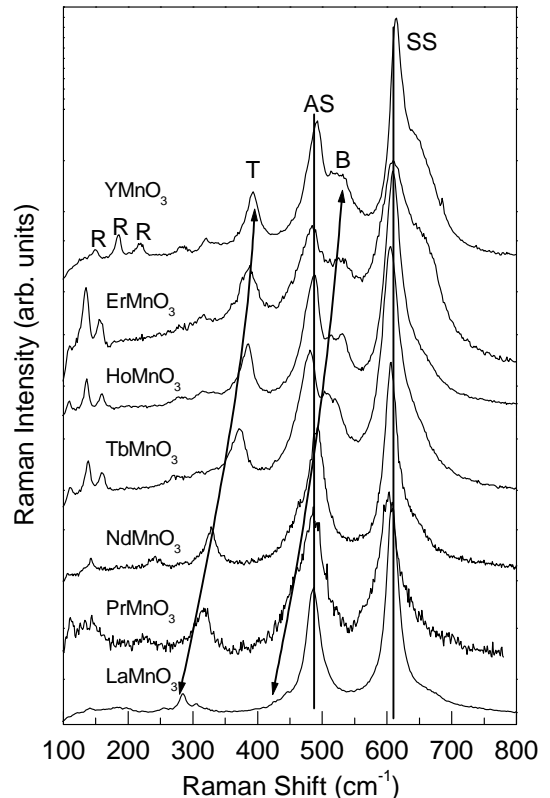


FIG. 1. Raman spectra at RT of Pbnm  $\text{RMnO}_3$  pellets.  $\text{LaMnO}_3$  is a single crystal. Same phonons in the spectra are connected with vertical lines. R: R ion modes, T: tilt, B: bending, and AS: antisymmetric and SS: symmetric stretching.

#### A. Compounds with strong cooperative Jahn-Teller distortion: $\text{RMnO}_3$

We have analyzed the Raman spectra at room temperature of orthorhombic  $\text{RMnO}_3$  compounds as a function of the chemical pressure by changing the rare earth ion (Fig. 1). There is agreement between all authors in the assignment of the peak around  $610 \text{ cm}^{-1}$ , related to a symmetric stretching of the basal oxygen ions of the octahedra ( $\text{B}_{1g}$ ), and that around  $280 \text{ cm}^{-1}$ , related to some octahedra tilt, but there are several claims concerning the one around  $480 \text{ cm}^{-1}$  and some confusion in the bending, tilt and rock modes in doped compounds<sup>6,11,15</sup>.

We assigned the  $480\text{ cm}^{-1}$  peak to an antisymmetric stretching ( $A_g$ ) associated with the JT distortion<sup>13,14</sup> and give here further evidence. Regarding tilt and bending modes, different combinations of displacements of the in plane O(2) ions along z axis and of the apical O(1) oxygen perpendicular to it, give rise to four tilt modes ( $A_g + B_{1g}$ ) and ( $B_{2g} + B_{3g}$ ) and two bending modes ( $A_g + B_{1g}$ ). We have grouped in brackets the Raman modes that may have very similar frequencies because they correspond to the same movements around x or y-axis. Raman spectra corresponding to modes with  $B_{2g}$  and  $B_{3g}$  symmetries have a very low intensity<sup>11</sup>, so we will focus on  $A_g$  and  $B_{1g}$  modes. The peaks at the lowest energies (marked with R in Fig.1) correspond to rare earth movements. Table I collects the measured frequencies together with the values estimated for the three R modes ( $\omega_R = \omega_Y \sqrt{M_Y/M_R}$ ) considering only the effect of the R mass and taking Y compound frequencies as references. The three R modes behave exactly as expected in all measured compounds. The differences between estimated and measured frequencies are lower than  $2\text{ cm}^{-1}$  except for  $\text{LaMnO}_3$  (6 and  $9\text{ cm}^{-1}$ ), due to the increase of La-O(1) distances compared to Y-O(1) ones.

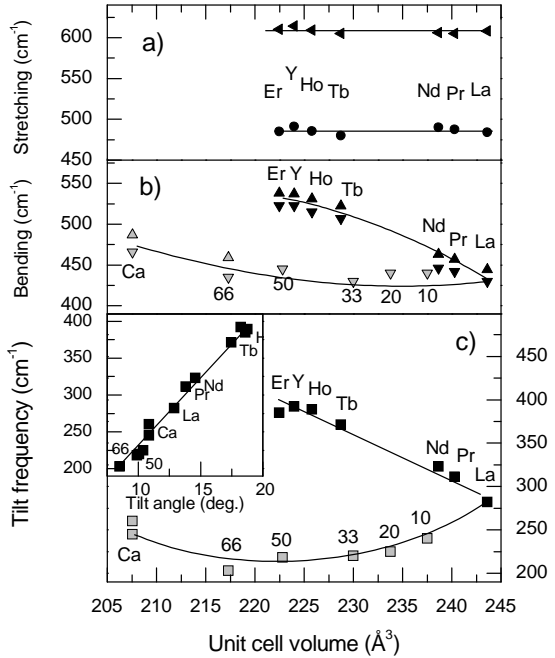


FIG. 2. Dependencies, vs the unit cell volume, of the RT frequencies of the symmetric and antisymmetric stretching modes a), bending modes b) and tilt mode c) for  $\text{RMnO}_3$  (black symbols) and  $\text{La}_{1-x}\text{Ca}_x\text{MnO}_3$  series (grey symbols). The numbers in the figure indicate the percentage of Ca doping. The inset shows the linear dependence of the tilt mode frequency with the tilt angle, which is defined as  $(180 - (\text{Mn-O}(1)-\text{Mn})) / 2$

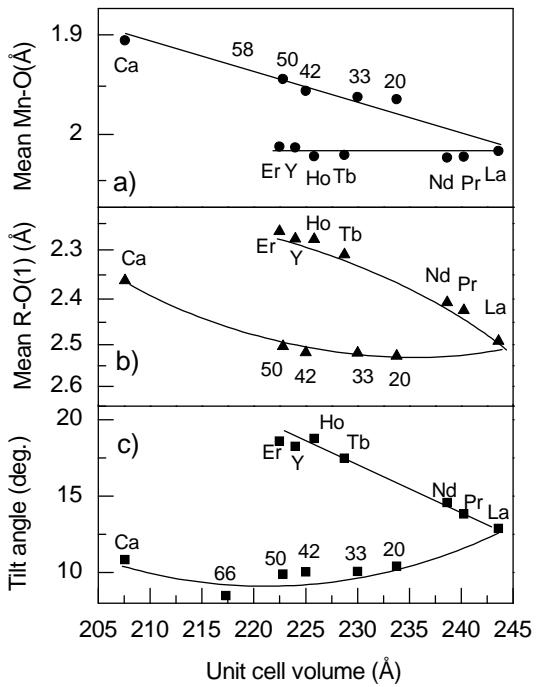


FIG. 3. Dependencies, vs the unit cell volume, of mean Mn-O distances a), mean R-O(1) distances b) and the octahedra tilt angle (defined as  $(180 - (\text{Mn-O}(1)-\text{Mn})) / 2$ ) c) for  $\text{RMnO}_3$  (structural data from Refs. 18 and 19) and  $\text{La}_{1-x}\text{Ca}_x\text{MnO}_3$  series (structural data from Refs. 6 and 26-28). The numbers in the figure indicate the percentage of Ca doping.

In Fig. 1 the two most intense peaks ( $610$  and  $480\text{ cm}^{-1}$ ) vary only slightly (less than  $10\text{ cm}^{-1}$ ) with the rare earth (Fig. 2). The symmetric (around  $610\text{ cm}^{-1}$ ) and the antisymmetric, or Jahn-Teller, (around  $480\text{ cm}^{-1}$ ) stretching modes involve nearly pure Mn-O bond stretching therefore a simple  $(d\text{Mn-O})^{-1.5}$  dependence of these phonon frequencies is expected<sup>25</sup> and observed. This is an indication that the  $\text{MnO}_6$  octahedron volume and bonds are insensitive to quite large changes in the tolerance factor in perovskites when comparing compounds with the same Mn valence state (in this case  $3^+$ ). On the contrary, the frequencies of the peaks labelled with "B" and "T" increase strongly (over  $100\text{ cm}^{-1}$ ) when the cell volume shrinks (Fig. 2b and c). The behavior of these phonons is parallel to that of the mean value of the two shortest R-O(1) bonds and to the static octahedra tilt (deviation from the cubic structure defined as  $(180 - (\text{Mn-O}(1)-\text{Mn})) / 2$ ) respectively (Fig. 3b and c). We assign the "B" peaks (two peaks can be distinguished) to bending modes ( $A_g + B_{1g}$ ) and the "T" peak to ( $A_g + B_{1g}$ ) tilt modes. The tilt and bending modes with  $A_g$  symmetry, that correspond to rotations around y-axis, are plotted in Fig. 4a and Fig. 4b, respectively. The  $B_{1g}$  modes correspond to the same atomic movements but around x-axis, therefore  $A_g$  and  $B_{1g}$  modes are expected to be very similar in frequency. The displacement of O(1) in

these modes is, in fact, a stretching of R-O(1) bonds (Fig. 4c). Each O(1) ion is surrounded by four R ions with two short and two long distances. Fig. 3b displays the evolution of the mean value of the two short R-O(1) bonds. Comparing Fig. 2b and Fig. 3b the correlation between

account the much shorter Mn-O distances their frequencies would be around 520 and 660  $\text{cm}^{-1}$ . We assign these quite sharp peaks to the bending ( $A_g = 487 \text{ cm}^{-1}$ ,  $B_{1g} = 466 \text{ cm}^{-1}$ ) and tilt ( $A_g = 245 \text{ cm}^{-1}$ ,  $B_{1g} = 260 \text{ cm}^{-1}$ ) modes ( $A_g$  modes are plotted in Fig. 4). The frequencies and relevant structural parameters of Ca doped series are presented in Fig. 2 and Fig. 3 making obvious their parallel behavior and confirming the modes assignment.

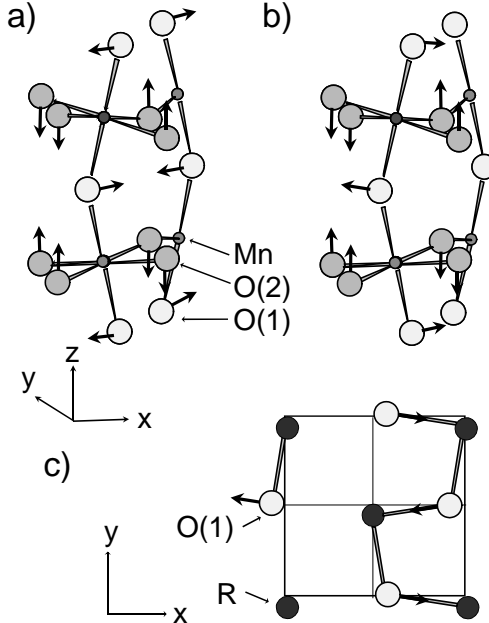


FIG. 4. a)  $A_g$  Octahedra tilt mode, b) and c)  $A_g$  octahedra bending mode. Both in the Pbnm structure.

In summary, the present data show that stretching mode frequencies correlate to Mn-O bond distances while the R-O bond and octahedra tilt angle dominate bending and tilt modes, respectively. These are the expected behaviors for such normal modes and must be kept in mind when trying to assign the spectra of doped or related compounds.

#### B. Insulating paramagnetic $\text{La}_{1-x}\text{Ca}_x\text{MnO}_3$ from $x=0$ to $x=1$

$\text{CaMnO}_3$  is also described with the Pbnm space group but with important differences compared to the previous  $\text{RMnO}_3$  compounds, that are the clues to understand their very different Raman spectra (Fig. 5c, 0% and 100% spectra). The Mn valence state is 4+ therefore no static nor dynamic JT distortions are present since the 3d  $e_g$  Mn orbital is empty.  $\text{CaMnO}_3$  cannot be described with the cubic perovskite structure because the tilt of the octahedra remains. The two pairs of peaks (around 240  $\text{cm}^{-1}$  and 460  $\text{cm}^{-1}$ ) cannot correspond to stretching modes (the dominant ones in  $\text{RMnO}_3$  ). Taking into

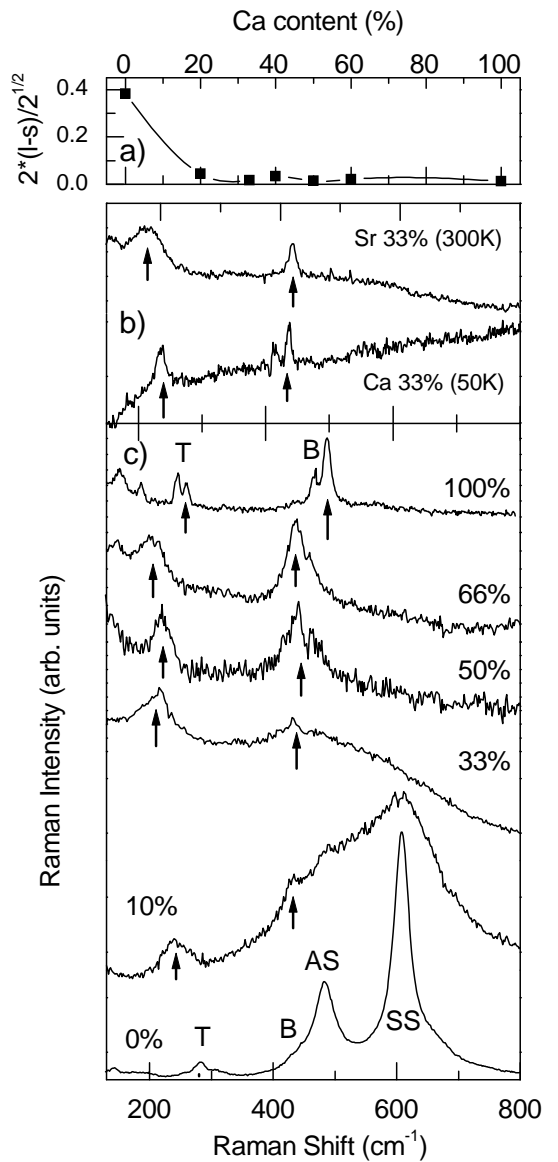


FIG. 5. a) Cooperative static JT distortion, from diffraction data in Refs. 16, 20-22, for  $\text{La}_{1-x}\text{Ca}_x\text{MnO}_3$  series; b) Raman spectra of FM metallic Ca (50K) and Sr (300K) doped  $\text{LaMnO}_3$  with  $x=0.33$ ; c) RT Raman spectra of  $\text{La}_{1-x}\text{Ca}_x\text{MnO}_3$  samples, as function of Ca content. The arrows point the narrow peaks corresponding to the tilt and bending modes.

During the referee process, a study of the Raman spectra of  $\text{CaMnO}_3$  appeared<sup>16</sup>. These authors assigned the

doublet at 242 and 258  $\text{cm}^{-1}$  to  $A_g$  and  $B_{2g}$  modes involving O (1) and Ca vibrations in the  $xz$  plane (in the Pnma representation that correspond to  $A_g$  and  $B_{1g}$  modes and  $xy$  plane in Pbnm one), and the 184  $\text{cm}^{-1}$  peak to the  $A_g$  tilt mode. Looking at Table I, the R modes in  $\text{CaMnO}_3$  are expected at 220, 274 and 325  $\text{cm}^{-1}$  and, in fact, two peaks of the correct symmetries are observed at 278<sup>16</sup> and 322  $\text{cm}^{-1}$  (Fig. 5c and Ref. 16). The Ca-O1 distances are similar to Y-O1 ones, consequently, the rule that has been found to be valid for all  $\text{RMnO}_3$  series should be valid for Ca compound. Therefore, the peaks at 242 and 259  $\text{cm}^{-1}$ , that show differences compared to the expected values over 22  $\text{cm}^{-1}$  (Table I), are not R modes. These peaks correspond to oxygen tilt modes. In a first approximation, as the unit cell volume decreases, the frequencies of all modes are expected to increase because the bonds shrink. The reason for the tilt modes to decrease is due to the reduction of the tilt angle as shown in the inset of Fig.2.

Fig. 5c collects the Raman spectra of LCMO compounds for several doping levels. Very significant changes are observed. Compared to stoichiometric  $\text{LaMnO}_3$ , for doping levels as low as 10%, the width of the stretching modes increases and their spectral weight decreases dramatically with doping. At 50% Ca doping and above no stretching modes appear and the spectra resembles strongly to the  $\text{CaMnO}_3$  one.

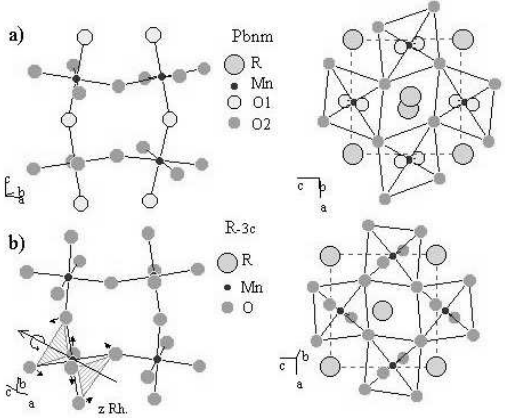


FIG. 6. Pbnm orthorhombic (a) and rhombohedral  $\text{R}\bar{3}\text{c}$  (b)  $\text{RMnO}_3$  structures. The rhombohedral axes have been rotated in order to better visualize the similarities between the octahedra network in both structures. The  $A_{1g}$  tilt mode is shown.

It is important to note that paramagnetic  $\text{CaMnO}_3$ , highly doped compounds (Fig. 5c) and the ferromagnetic metallic phase of  $\text{La}_{0.67}\text{Ca}_{0.33}\text{MnO}_3$  (Fig. 5b) present very similar Raman spectra. These quite different systems have in common that the cooperative JT distortion is negligible (Fig. 5a) and that they do not present the stretching modes. We can conclude that a JT distortion, or probably a distortion engendering significantly differ-

ent Mn-O bond lengths, is necessary to produce a measurable intensity of the stretching modes. The allowed modes by global symmetry considerations are identical to the previous  $\text{RMnO}_3$  compounds but the change in the polarizability due to a particular mode, that determines its Raman intensity, is found to vanish for the stretching modes of the regular octahedra.

On the other hand, these spectra are nearly identical to that corresponding to rhombohedral  $\text{La}_{0.7}\text{Sr}_{0.3}\text{MnO}_3$  (Fig. 5b). The observable Raman active modes of the  $\text{R}\bar{3}\text{c}$  structure correspond to bending and tilt modes of the oxygen octahedra, whose atomic displacements are very similar to the bending and tilt modes of the orthorhombic structure (see tilt mode in Figs. 4a and 6b). From  $\text{R}\bar{3}\text{c}$  to Pbnm the number of expected peaks increases. Only one bending  $E_g$  and two tilt modes ( $A_{1g} + E_g$ ) are expected in the  $\text{R}\bar{3}\text{c}$  rhombohedral structure while four bending and four tilts modes correspond to the orthorhombic Pbnm one. As shown in Fig. 6, the octahedra network in the Pbnm and  $\text{R}\bar{3}\text{c}$  structures are very similar. Both present tilted octahedra with similar angles (about 160° for  $\text{R}\bar{3}\text{c}$ ) but Pbnm structure can present up to three different Mn-O distances, while all Mn-O bond lengths are identical in the rhombohedral one. But highly doped Ca compounds, as well as the metallic phases of Ca and Sr doped compounds, do not present cooperative or dynamic JT distortions. In these cases the octahedra in Pbnm and  $\text{R}\bar{3}\text{c}$  space groups are almost identical. Even if the stretching modes are allowed by symmetry in the Pbnm space group, the origin of the close similarity of their spectra, in particular the absence of high frequency modes, becomes clear.

We conclude therefore that there are two spectra type, one corresponding to compounds with a cooperative JT distortion ( $\text{LaMnO}_3$  type) that is dominated by the stretching phonons, and the other without these modes corresponding to compounds without JT distortion, like  $\text{CaMnO}_3$ , metallic Pbnm phases or rhombohedral LSMO.

### C. Paramagnetic phases of low to optimally doped manganites

At low doping levels, for example  $\text{La}_{0.9}\text{Ca}_{0.1}\text{MnO}_3$  in Fig 5c or  $\text{RMnO}_{3-\delta}$ , ( $\text{R}=\text{La}$  or  $\text{Pr}$ ) in Fig. 7, the spectra are similar to  $\text{LaMnO}_3$  one but with wider peaks. The dynamic fluctuations of the octahedra caused by the lattice polaron hopping increase very substantially their width. But  $\text{La}_{0.66}\text{Ca}_{0.33}\text{MnO}_3$  (LCMO) or  $\text{La}_{0.9}\text{MnO}_3$  (Fig. 7) present some spectral weight in the stretching frequency range (AS and SS) together with narrower peaks (indicated with arrows). In order to check whether these peaks have the same origin as the broad high frequency bands, we compare their spectra to the undoped  $\text{LaMnO}_3$  at  $T>800\text{K}$  (lower spectrum in Fig. 7) above the so-called JT transition. At these temperatures, the cooperative JT distortion is melted but dynamical JT

fluctuations remain<sup>14,19</sup>. This is a very similar scenario to what occurs in the paramagnetic phase of LCMO, therefore similar Raman spectrum would be expected. Fig. 7 shows that above 800 K the intensity has decreased drastically compared to RT spectrum (Fig. 5) but some spectral weight is observable in the high frequency region corresponding to the stretching modes while tilt and bending modes have almost vanished. It is evident that dynamic distortions of the  $MnO_6$  octahedra cannot give rise to the quite narrow peaks around 230 and 420  $cm^{-1}$ , but are the origin of the broad stretching bands.

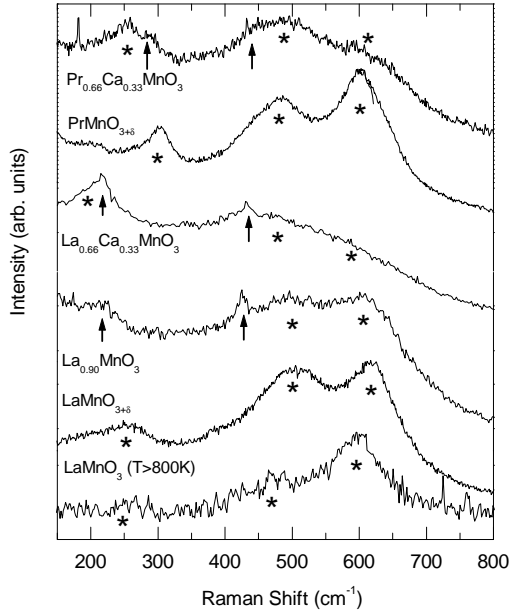


FIG. 7. Raman spectra at RT of non-stoichiometric  $RMnO_3$  ( $R=La$  and  $Pr$ ) as well as 33% Ca doped compounds. Bottom: Raman spectrum of  $LaMnO_3$  at  $T>800K$  above the JT transition. Small arrows point the narrow peaks related to the  $R\bar{3}c$  type phase and the stars position the modes associated with the  $Pbnm$  type phase with dynamic and/or cooperative JT distortion.

Doping  $LaMnO_3$  gives rise Mn valence mixing and local static distortions around the doping ion. Simultaneously, in the paramagnetic phase, the hopping electrons trapped as lattice polarons induce lattice distortions. This disorder is of dynamic character and is expected to change at the insulator to metallic phase transition and has been described as a crossover from small to large polaron regimes<sup>8</sup>. Diffraction techniques give us valuable information on the mean interatomic distances but not on instantaneous or randomly distributed atomic positions, which are important for the Raman scattering effect. The analysis of the diffuse X-ray scattering<sup>29</sup> and Reverse Monte-Carlo simulations of neutron diffraction patterns<sup>30,31</sup> have shown that local octahedron distortions are much larger, around and above  $T_c$ , than the obtained by standard diffraction analysis. Diffraction

shows very slight structural changes at the ferromagnetic metallic transition while Raman spectra above (Fig. 5c) and bellow (Fig. 5b)  $T_c$  are quite different. Above  $T_c$ , the features similar to high temperature  $LaMnO_3$  correspond to the paramagnetic matrix dynamically distorted by polaron hopping, and the ones similar to  $CaMnO_3$  spectrum indicate that part of the sample has a structure alike the metallic ferromagnetic phase. It might correspond to the magnetic clusters or magnetic polarons that have been observed by different techniques<sup>32</sup>. The structure of these entities is unknown but present ferromagnetic correlations. In the present knowledge of phase segregation or inhomogeneous intrinsic phase, present in most of the manganites, it is realistic to think that the second spectrum corresponds to ferromagnetic metallic droplets in the paramagnetic matrix with polaronic (lattice polarons) conduction. At low temperatures, well in the metallic regime, only the narrow peaks, similar to  $CaMnO_3$ , remain.

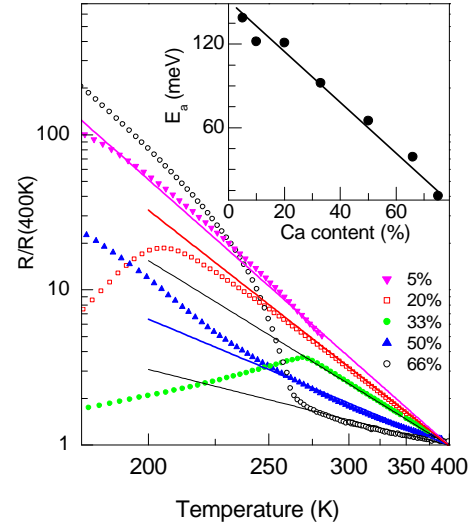


FIG. 8. Normalized resistance of samples with several Ca content. Lines are fits to the paramagnetic state resistance with:  $R=R_0 \exp(E_a/K_B T)$ . The inset shows the obtained activation energies  $E_a$  vs Ca content.

The coexistence of the two types of spectra, related to two phases or micro-phases, is observed in several compounds in Fig. 5c and Fig. 7 and, for example, in Fig. 1b of Ref. 16. In fact, in the present scenario we can understand the temperature dependence of spectra from Ref. 17. Compounds with  $x=0.2$  and  $0.1$  are both paramagnetic insulators (PMI) at high temperatures. The  $x=0.2$  one becomes ferromagnetic (FM) and metallic at 280K while  $x=0.1$  transforms in a FM insulator at 200K. The temperature dependence of  $La_{0.8}Sr_{0.2}MnO_3$  spectrum is "identical" to the changes observed in  $La_{0.67}Ca_{0.33}MnO_3$ , in spite of their different average structures ( $R\bar{3}c$  and  $Pbnm$ , respectively). In the insulating paramagnetic phases, dynamically distorted octahedra ( $Pbnm$  type) co-

exist with regular octahedra ( $R\bar{3}c$  type) while in the ferromagnetic metallic regime only regular octahedra remain. On the contrary, in  $x=0.1$  Sr doped  $\text{LaMnO}_3$ , above  $T_c$ , only the broad features are observed corresponding to the  $\text{Pbnm}$  structure with dynamic distortions related to polaron hopping. But, below  $T_c$ , the appearance of narrow peaks, in coexistence with the broad bands, indicates that metallic, and probably ferromagnetic, clusters in the insulating matrix are formed. In the discussion about the nature of the FMI phase of this  $x=0.1$  compound, on whether it is a canted ferromagnetic or phase segregation is occurring, Raman spectrum is consistent with the second hypothesis. Nevertheless a more detailed analysis is necessary.

When Ca content increases the binding energy of the lattice polarons decreases, as indicates the reduction of the activation energy for conduction in the paramagnetic phase (Fig. 8). The reduction of the polaron energy implies the collapse of the amplitude of the dynamic distortions it produces in the lattice and, therefore, of the spectral weight of the  $\text{LaMnO}_3$  type spectrum. The width of the instantaneous distribution of Mn-O distances is the origin of the width of the Raman peaks. For doping concentrations of 50% and above the lattice is in fact, instantaneously, much more regular than at low doping. We recover the  $\text{CaMnO}_3$  or  $\text{LSMO}$  type spectrum. In the metallic regime, the hopping carriers become delocalized and do not induce lattice distortions. Sharp phonon peaks are observed below  $450 \text{ cm}^{-1}$  independently of the crystallographic structure (compare metallic  $\text{Pbnm}$   $\text{LCMO}$  and metallic  $R\bar{3}c$   $\text{LSMO}$  at RT (Fig. 5b) and at low temperature<sup>33</sup>). Therefore, the width and intensity of the stretching modes are a measure of the amplitude of the dynamical JT distortions which correlates to the activation energy for polaronic conduction.

At last, the main characteristic of the Raman spectra of most charge ordered phases, that is the recovery of the stretching phonon peaks, is understood as being caused by the orbital order and the concomitant cooperative JT distortion.

## V. CONCLUSIONS

The analysis of the Raman spectra of  $\text{RMnO}_3$   $\text{Pbnm}$  compounds that present strong cooperative JT distortion show that the stretching modes (symmetric and antisymmetric) correlate to Mn-O bonds while bending modes are determined by the R-O(1) mean distance and tilt modes by Mn-O-Mn angle. Compounds without cooperative or dynamic distortions of the  $\text{MnO}_6$  octahedra, independently of their mean crystallographic structure, do not present stretching modes and the characteristics of their spectra can be approached to the  $R\bar{3}c$  space group vibrations. The bending and tilt normal modes are equivalent to the  $\text{Pbnm}$  ones and the measured frequencies follow the same rules as  $\text{RMnO}_3$  ones. This explains the

similarities between insulating  $\text{CaMnO}_3$  ( $\text{Pbnm}$ ) and the metallic phases of orthorhombic  $\text{La}_{0.67}\text{Ca}_{0.33}\text{MnO}_3$  and rhombohedral  $\text{La}_{0.67}\text{Sr}_{0.33}\text{MnO}_3$ . The activation energy for conduction in the insulating phases, which is proportional to the polaron binding energy, is a measure of the amplitude of the dynamic distortion it produces in the lattice. Therefore, as the Ca content increases, the activation energy decreases as well as the amplitude of the dynamic distortions. The width of the peaks corresponding to  $\text{RMnO}_3$  type spectrum increases and their intensity decreases as the Ca content rises up to about 50% where these peaks vanish and only the  $\text{CaMnO}_3$  type spectrum is observed. The identification of these types of spectra and their correspondence with particular octahedron configurations are the keys to understand the Raman spectra of most manganese perovskite. Moreover, this allows to detect the simultaneous presence of several different phases and to obtain insight in their local structure.

## ACKNOWLEDGMENTS

We wish to acknowledge the financial support from CICYT under contracts MAT2000-1384 and MAT2001-0539.

- 
- <sup>1</sup> S. Jin, T.H. Tiefel, M. McCormack, R.A. Fastnacht, R. Ramesh, L.H. Chen, *Science* 264, 413 (1994)
  - <sup>2</sup> M. Ziese, *Rep. Prog. Phys.* 65, 143 (2002)
  - <sup>3</sup> E. Dagotto, T. Hotta and A. Moreo, *Phys. Reports* 344, 1 (2001)
  - <sup>4</sup> Philip B. Allen and Vasili Perebeinos, *Phys. Rev. B* 60, 10747 (1999)
  - <sup>5</sup> J.C. Irwin, J. Chrzanowski and J.P. Franck, *Phys. Rev. B* 59, 9362 (1999)
  - <sup>6</sup> E. Liarokapis, Th. Leventouri, D. Lampakis, D. Palles, J.J. Neumeier and D.H. Goodwin, *Phys. Rev. B* 60, 12758 (1999)
  - <sup>7</sup> E. Granado, A. García, J.A. Sanjurjo, C. Rettori, I. Torriani, F. Prado, R.D. Sánchez, A. Caneiro and S.B. Oseroff, *Phys. Rev. B* 60, 11879 (1999)
  - <sup>8</sup> S. Yoon, H.L. Liu, G. Schollerer, S.L. Cooper, P.D. Han, D.A. Payne, S.W. Cheong and Z. Fisk, *Phys. Rev. B* 58, 2795 (1998)
  - <sup>9</sup> H.L. Liu, S. Yoon, S.L. Cooper, S.W. Cheong, P.D. Han and D.A. Payne, *Phys. Rev. B* 58, 10115 (1998)
  - <sup>10</sup> M.R. Ibarra, Guo-meng Zhao, J.M. De Teresa, B. García-Landa, Z. Arnold, C. Marquina, P.A. Algarabel, H. Keller and C. Ritter, *Phys. Rev. B* 57, 7446 (1998)
  - <sup>11</sup> M.N. Iliev, M.V. Abrashev, H.G. Lee, V.N. Popov, Y.Y. Sun, C. Thomsen, R.L. Meng and C.W. Chu, *Phys. Rev. B* 57, 2872 (1998)

- <sup>12</sup> V.B. Podobedov, A. Weber, D.B. Romero, J.P. Rice, H.D. Drew, Phys. Rev. B 58, 43 (1998)
- <sup>13</sup> L. Martín-Carrón, A. de Andrés, M.T. Casais, M.J. Martínez-Lope and J.A. Alonso, J. Alloys and Compounds 323-324, 494 (2001)
- <sup>14</sup> L. Martín-Carrón and A. de Andrés, The Europ. Phys.J. B 22, 11 (2001); L. Martín-Carrón and A. de Andrés, J. Alloys and Compounds 323-324, 417 (2001)
- <sup>15</sup> V. A. Amelichev, B. Gütler, O. Yu. Gorbenko, A. R. Kaul, A. A. Bosak and A. Yu. Ganin, Phys. Rev. B, 63, 104430 (2001)
- <sup>16</sup> M. V. Abrashev, J. Bäckström, L. Börjesson, V. N. Popov, R. A. Chakalov, N. Kolev, R.-L. Meng and M. N. Iliev, Phys. Rev. B, 65, 184301 (2002)
- <sup>17</sup> P. Björnsson, M. Rüthausen, J. Bäckström, M. Käll, S. Eriksson, J. Eriksen, L. Börjesson, Phys. Rev. B 61, 1193 (2000)
- <sup>18</sup> J.A. Alonso, M.J. Martínez-Lope, M.T. Casais and M.T. Fernández-Díaz, Inorg. Chem. 39, 917 (2000)
- <sup>19</sup> J. Rodríguez-Carvajal, M. Hennion, F. Moussa, A.H. Moudden, L. Pinsard and A. Revcolevschi, Phys. Rev. B 57 R3189, (1998)
- <sup>20</sup> J.A. Alonso, M.J. Martínez-Lope, M.T. Casais, J.L. MacManus-Driscoll, P.S.I.P.N. de Silva, L.F. Cohen and M.T. Fernández-Díaz, J. Mater. Chem. 7, 2139 (1997)
- <sup>21</sup> J.A. Alonso, Phil. Trans. R. Soc. Lond. A 356, 1617 (1998)
- <sup>22</sup> A. Urushibara, Y. Moritomo, T. Arima, A. Asamitsu, G. Kido and Y. Tokura, Phys. Rev. B 51, 14103 (1995)
- <sup>23</sup> K. R. Poeppelmeier, M. E. Leonowicz, J. C. Scanlon, J.M. Longo and W. B. Yelon, J. Solid State Chem. 45, 71 (1982)
- <sup>24</sup> M.V. Abrashev, A.P. Litvinchuk, M.N. Iliev, R.L. Meng, V.N. Popov, V.G. Ivanov, R.A. Chakalov and C. Thomsen, Phys. Rev. B 59, 4146 (1999)
- <sup>25</sup> A. de Andrés, S. Taboada, J.L. Martínez, A. Salinas, J. and R. Sáez-Puche. Phys. Rev. B 47, 14898-14904 (1993).
- <sup>26</sup> P. Dai, J. Zhang, H.A. Mook, S-H. Liou, P.A. Dowben and E.W. Plummer, Phys. Rev. B 54, R3694 (1996)
- <sup>27</sup> P.G. Radaelli, D.E. Cox, M. Marezio and S-W. Cheong, Phys. Rev. B 55, 3015 (1997)
- <sup>28</sup> S. Faaland, K.D. Knudsen, M.A. Einarsrud, L. Rørmark, R. Høier and T. Grande, J. Solid State Chem. 140, 320 (1998)
- <sup>29</sup> S. Shimomura, N. Wakabayashi, H. Kuwahara and Y. Tokura, Phys. Rev. Lett. 83, 4389 (1999)
- <sup>30</sup> D. Louca and T. Egami, Phys. Rev. B 59, 6193 (1999)
- <sup>31</sup> M. García-Hernández, A. Mellergård, F.J. Mompean, D. Sánchez, A. de Andrés, R.L. McGreevy and J.L. Martínez, cond-mat/0201436
- <sup>32</sup> J.M De Teresa, M.R. Ibarra, P.A. Algarabel, C. Ritter, C. Marquina, J. Blasco, J. García, A. del Moral and Z. Arnold, Nature (London) 386, 256 (1997)
- <sup>33</sup> E. Granado, N.O. Moreno, A. García, J.A. Sanjurjo, C. Rettori, I. Torriani, S.B. Oseroff, J.J. Neumeier, K.J. McClellan, S.W. Cheong, Y. Tokura, Phys. Rev. B 58, 11435 (1998)

TABLE I. Observed and estimated R modes frequencies for RMnO<sub>3</sub> compounds. The estimated values have been obtained with  $\omega_R = \omega_Y \sqrt{M_Y/M_R}$ . TW stands for "this work". (\*) this peak is assigned in Ref. 16 to a R mode (A<sub>g</sub> symmetry)

assignment	Ca (40)			Y (89)		La (139)		Nd (144)		Tb (159)		Ho (165)		Er (167)	
	Est.	TW	Ref. 15	TW	Ref. 11	Est.	TW								
A <sub>g</sub> /B <sub>1g</sub>	220	-	242/259	148	151/151	118	109	116.5	-	110.5	111	108.8	109	108	-
A <sub>g</sub>	274	-	278	184	188	147	141	144.9	143	137	138	135.2	136	134	134
B <sub>1g</sub>	325	322	322*	218	220	174		171.6	-	162.5	160	160.3	160	159.1	157